Structural, optical, and electrical properties of Cu-doped ZrO_2 films prepared by magnetron co-sputtering*

Nian-Qi Yao(姚念琦), Zhi-Chao Liu(刘智超), Guang-Rui Gu(顾广瑞)†, and Bao-Jia Wu(吴宝嘉)

Department of Physics, College of Science, Yanbian University, Yanji 133002, *China*

(Received 10 April 2017; revised manuscript received 27 June 2017; published online 20 August 2017)

Copper (Cu)-doped ZrO_2 (CZO) films with different Cu content (0 at.%∼ 8.07 at.%) are successfully deposited on Si (100) substrates by direct current (DC) and radio frequency (RF) magnetron co-sputtering. The influences of Cu content on structural, morphological, optical and electrical properties of CZO films are discussed in detail. The CZO films exhibit ZrO_2 monocline ($\bar{1}11$) preferred orientation, which indicates that Cu atoms are doped in ZrO_2 host lattice. The crystallite size estimated form x-ray diffraction (XRD) increases by Cu doping, which accords with the result observed from the scanning electron microscope (SEM). The electrical resistivity decreases from 2.63 Ω.cm to 1.48 Ω·cm with Cu doping content increasing, which indicates that the conductivity of CZO film is improved. However, the visible light transmittances decrease slightly by Cu doping and the optical band gap values decrease from 4.64 eV to 4.48 eV for CZO films.

Keywords: Cu-doped ZrO_2 films, magnetron co-sputtering, resistivity, transmittance

PACS: 68.55.A–, 73.61.–r, 78.66.–w, 81.15.Cd **DOI:** 10.1088/1674-1056/26/10/106801

1. Introduction

Transition metal oxide thin film, especially ZrO_2, is a great active material due to its versatile nature, such as high chemical inertness, photochemical stability, good wear resistance, and wide band gap. Because of these properties, ZrO_2 film is extensively applied to many fields, such as fuel cells, optical coatings, radiation shielding.[1–4] In particular, ZrO_2 thin film is a promising alternative to SiO_2 as the high κ gate dielectric in complementary metal–oxide–semiconductor technology, due to its high dielectric constant, wide energy band and offsets, and good stability with Si surface.[5–9] It is known that ZrO_2 has three stable structures. The ZrO_2 has monoclinic structure (m-ZrO_2) at room-temperature, and it is transformed into a tetragonal structure (t-ZrO_2) in a temperature range from 950 °C to 1170 °C and cubic structure (c-ZrO_2) over 1170 °C.[10,11] The structure and properties of ZrO_2 film strongly depend on the deposition technique and growth condition. Many researchers have tried different methods to deposit ZrO_2 films, such as thermal decomposition,[12] electron-beam evaporation,[13] chemical vapor deposition,[14,15] sol–gel method,[16] reactive sputtering,[17,18] etc. Among these methods, sputtering is known as a technique which has many merits suitable for industrial applications, such as easily depositing film in a large area, simple apparatus, low substrate temperature, high deposition rate, good adhesion to the substrate, etc.[19,20]

As is well known, the addition of several elements such as Al,[21] Au,[16] Fe,[22] Tb,[23] Er,[24] etc. into ZrO_2 film is a very effective method to influence its structure and phase composition and thereby its properties. To the best of our knowledge, there is little research about the preparation of Cu-doped ZrO_2. Additionally, Cu in its Cu^{2+} ionic state has an ionic radius (0.72 Å) similar to that of Zr^{4+} (0.8 Å) and the similarities in their electronic structure, so Cu^{2+} ions can dope easily into the ZrO_2 host lattice. Thus, we are to prepare Cu-doped ZrO_2 (CZO) films with high crystalline quality and investigate the effects of Cu doping on the structural, morphological, electrical, and optical properties in this paper.

2. Experimental details

CZO films for various doping content of Cu (0, 5.93, 7.18, and 8.07 at.%) were deposited on Si (100) and glass substrates by DC and RF magnetron co-sputtering. Zr target (pure, 99.99%) and Cu target (pure, 99.99%) were employed as source materials. All the RF depositions were performed at a fixed RF sputter power of 100 W applied to the Zr target. In order to produce CZO films with different Cu content, the DC sputtering power applied to the Cu target was varied from 0 W to 70 W. The substrate holder was fixed to a distance of 6 cm from the sputter targets and the substrate temperature was maintained around 600 °C. Prior to installing the substrates into the deposition chamber, they were ultrasonically cleaned in acetone, alcohol and deionized water for 20 min, then blown dry with purified nitrogen gas. The sputtering chamber was evacuated to a base pressure of 5×10^{-4} Pa using rotary and turbo molecular pump combination and the working pressure was set to be 2.0 Pa. High pure argon (99.99%) and high pure oxygen (99.99%) as working gas were introduced into the sputter chamber through mass flow controllers with Ar and O_2 flow rates being 50 sccm and 30 sccm, respectively. In order

*Project supported by the National Natural Science Foundation of China (Grant Nos. 51272224 and 11164031).

†Corresponding author. E-mail: grgu@ybu.edu.cn

© 2017 Chinese Physical Society and IOP Publishing Ltd

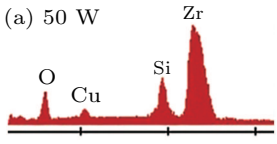
to improve the crystalline quality and remove other contaminants present on the target surface, the pre-sputtering process was carried out for 15 min in argon atmosphere.

Various characterization techniques have been performed to study the influences of CZO films. The crystal structures of samples were characterized by x-ray diffraction (TonDa, Td-2500) using Cu Kα radiation ($\lambda = 1.5406$ Å). The chemical composition and surface morphology of CZO films were characterized by energy dispersive x-ray spectroscopy (EDX) and field emission scanning electron microscope (SEM) (FEI XL-30). The electrical resistivities of films were measured by using four-point probe technique (SZT-2A). Optical transmission spectra of the films were recorded in a specific wavelength range from 200 nm to 800 nm by using UV–vis NIR spectrophotometer (Shimadzu, UV-3600). All the measurements were performed at room temperature.

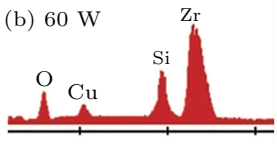
3. Results and discussion

3.1. Elemental composition

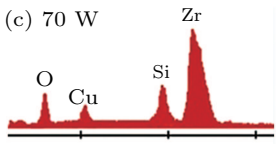
The Cu atom concentration in the CZO films has been identified by EDX analysis and presented in Fig. 1. As shown in EDX spectra, it can be confirmed that the deposited films are associated with characteristic Zr and O elements indicated by the high intensity peaks, whereas the low intensity peak attributed to Cu doping is evidence for the minor composition of Cu to be incorporated into ZrO_2 film. Figures 1(a)–1(c) show the EDX spectra of CZO films with Cu content of 5.93, 7.18, and 8.07 at.%, respectively. The observed Cu content in ZrO_2 film increases from 0 at.% to 8.07 at.% with the increase of DC sputter power from 0 W to 70 W.



Element	wt%	at.%
OK	26.36	60.22
CuL	10.32	5.93
SiK	9.41	12.24
ZrL	53.92	21.6
Total	100	100



Element	wt%	at.%
OK	26.13	60.25
CuL	12.37	7.18
SiK	8.47	12.13
ZrL	53.03	21.44
Total	100	100



Element	wt%	at.%
OK	26.63	60.44
CuL	14.13	8.07
SiK	8.84	14.42
ZrL	50.4	20.06
Total	100	100

Fig. 1. (color online) EDX spectra of CZO films formed at Cu content of (a) 5.93 at.%; (b) 7.18 at.%, and (c) 8.07 at.%.

3.2. Structural properties

Figure 2 shows the x-ray diffraction (XRD) patterns of the CZO films deposited on Si (100) substrates. From the XRD results, it is seen that all deposited films exhibit the ($\bar{1}11$) high intensity crystalline peak corresponding to ZrO_2 monoclinic, which is in good agreement with the data of the standard JCPDS card No. 37-1484. When Cu-doping content is increased from 0 at.% to 7.18 at.%, the additional secondary peaks corresponding to Cu atom clusters or diverse metal oxides evidently disappear, which could be due to the homogenous mixing of Cu in the matrix of ZrO_2, indicating the perfect solubility of Cu into ZrO_2 host lattice. Moreover, the intensities of all peaks do not change much with Cu doping content increasing, indicating that the Cu^{2+} ions are perfectly incorporated into ZrO_2 host lattice, without affecting the crystallinity of the ZrO_2. However, when Cu-doping content is increased to 8.07 at.%, the intensity of ($\bar{1}11$) peak is weakened and a new diffraction peak is assigned to the copper oxide phase. Higher doping levels of Cu may energetically lead to coalescence of Cu atoms into metallic clusters. This observation is explained by the fact that Cu atoms first incorporate into the nanocrystal (50 W and 60 W) and then diffuse outward followed by the formation of crystalline CuO (70 W).[25,26] Mukhtar *et al.*[27] reported similar results that Cu-doped films have no secondary phases of Cu up to the moderate doping level of Cu 11 at.%. In addition, the full width at half maximum (FWHM) of preferential ZrO_2 ($\bar{1}11$) peak decreases with the increase of Cu content in ZrO_2 host lattice by substituting Cu^{2+} ions for Zr^{4+} ions. It can do so due to the ionic radius of Cu^{2+} (0.72 Å) being smaller than Zr^{4+} (0.8 Å) radius. It is also observed that with Cu content increasing, the location of the ($\bar{1}11$) diffraction peak shifts toward the high angle direction compared with that of the pure ZrO_2 films as shown in Fig. 2(b), indicating important evidence of replacement of Zr^{4+} with Cu^{2+} ions.

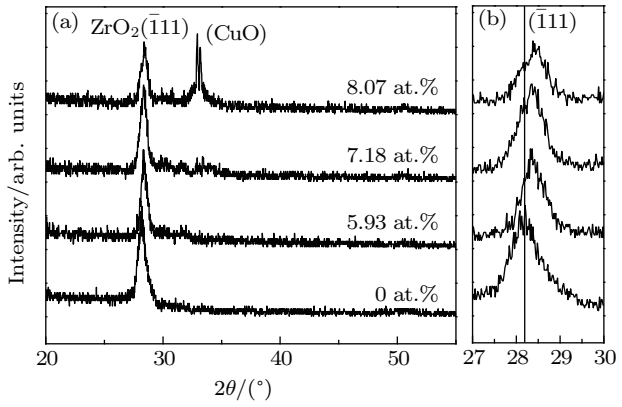


Fig. 2. (a) XRD patterns of CZO films formed at various Cu doping content, (b) the specific XRD patterns of ($\bar{1}10$) peak.

All films are evaluated by using the structural parameters such as crystallite size. The average crystallite sizes of the samples are estimated from the broadening of the diffraction peaks ($\bar{1}11$) using the Scherrer's formula[28]

$$D = \frac{K\lambda}{\beta \cos\theta}, \quad (1)$$

where D is the crystallite size, $K = 0.89$ the correction factor, λ the wavelength of the x-ray radiation (Cu Kα, $\lambda = 0.15405$ nm), β the corrected peak width at FWHM, and θ the Bragg angle. The calculated values including diffraction angle, FWHM, crystallite size of the Cu-doped ZrO_2 ($\bar{1}11$) diffraction peak are summarized in Table 1. From Table 1, it can be seen that the crystallite size of the films first increases and then decreases as the Cu content increases. The crystallite size increases from 12.5 nm to 15.1 nm with increasing Cu content from 0 at.% to 5.93 at.%. We can speculate that the increase of crystallite size with Cu doping is due to Cu^{2+} substituting for Zr^{4+}. However, further increasing Cu content to 8.07 at.%, the crystallite size slightly decreases to 13.2 nm. This may be attributed to the formation of stress by the difference in ionic size between Cu^{2+} (0.72 Å) and Zr^{4+} (0.8 Å) and the segregation of dopants in the grain boundaries for the higher doping content case. This can disturb the long-range crystallographic ordering, thereby reducing the crystallite size.[29]

Table 1. The values of Cu content, diffraction angle, FWHM, crystallite size of the CZO films.

Cu target power/W	Cu/at.%	2θ/(°)	FWHM	Crystallite size/nm
0	0	28.18	0.646	12.5
50	5.93	28.38	0.535	15.1
60	7.18	28.40	0.603	13.4
70	8.07	28.42	0.613	13.2

3.3. Morphological analysis

The surface morphologies of the films are further investigated by field emission scanning electron microscopy (SEM). Figures 3(a)–(3d) show the morphologies of CZO films deposited on Si (100) substrates at different Cu doping levels from 0 to 8.07 at.%, respectively. In Fig. 3(a), it can be observed that the pure ZrO_2 film exhibits continuously, uniformly and without micro-cracks while small particles can be observed from the surface. At a lower doping level (5.93 at.%), there is more and more impurity clustering, leading to the increase of grain size and the more obvious protuberance as shown in Fig. 3(b). The enhanced grain size and surface roughness with Cu doping may be ascribed to the formation of clusters due to the aggregation of smaller grains. Kumaravel *et al.*[30] has also reported that the increase of grain size with the roughness of film increasing is due to the increase of density and size of metal particles on the surface of the film. However, when the Cu content is more than 5.93 at.%, the grain size decreases as shown in Figs. 3(c) and 3(d). The trend in the variation of grain size is in good agreement with that of the crystallite size calculated from XRD. The CZO film has larger grain size and surface roughness than the pure ZrO_2 film, which indicates that the surface morphology is strongly influenced by the Cu-doping.

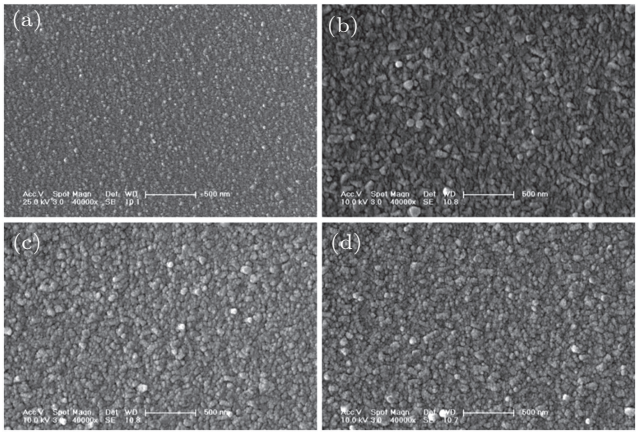


Fig. 3. Scanning electron microscopy (SEM) images of the Cu-doped ZrO_2 films formed at Cu content of (a) 0 at.%; (b) 5.93 at.%; (c) 7.18 at.%, and (d) 8.07 at.%.

3.4. Electrical properties

The variation of electrical resistivity of CZO film with Cu doping content is shown in Fig. 4. Four-point probe method is a routine method of measuring the resistivity of film, due to its simple operation, easily reading and calculating, and no damage to sample surface. The resistivity (ρ) of film can be calculated from the following equation:[31]

$$\rho = C\frac{V}{I}, \tag{2}$$

where $C \approx 6.28 \pm 0.05$ cm is the probe coefficient. We can improve measurement precision by averaging the testing values of repeated measurements (in Table 2). It could be seen from Fig. 4 that the electrical resistivity of CZO film is remarkably dependent on Cu doping content. The resistivity of CZO film is smaller than that of the pure ZrO_2 film, and first decreases then increases with Cu doping content increasing. The pure ZrO_2 film shows an electrical resistivity of 2.63 Ω·cm. At lower doping levels of Cu (5.93 at.% and 7.18 at.%), the resistivities of CZO film are about 1.78 Ω·cm and 1.48 Ω·cm, respectively. At a higher doping level of Cu 8.07 at.%, the resistivity increases to 2.57 Ω·cm. A similar trend of the variation in the electrical resistivity of Cu-doped film has been observed by Sreedhar *et al.*[32] The decrease of resistivity observed in

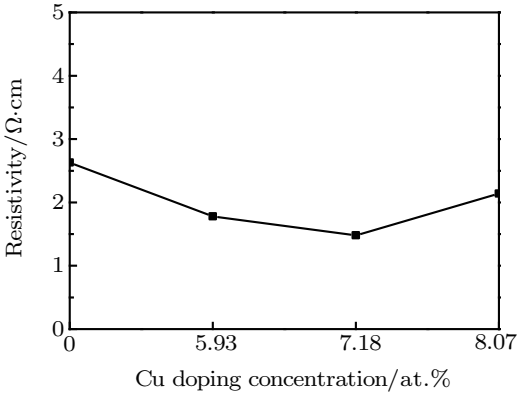


Fig. 4. Variation of electrical resistivity of the CZO film with Cu doping content.

the lower doped sample may be attributed to the holes transferring from Zr^{4+} ions to the Cu^{2+} ions located at the substitution sites, until ZrO_2 host lattices receive the maximum doping content of the Cu atoms. However, with the further increase of the Cu content (8.07 at.%), the resistivity is found to increase. The increase of the resistivity for a higher Cu doping content (8.07 at.%) may be due to the presence of the copper oxide, which can act as a scattering center, resulting in the increase of the resistivity. Presto *et al.*[33] reported the same results: the resistivity decreases with the Cu doping content increasing. However, as the CuO is added, the resistivity slightly increases.

Table 2. Values of Cu content, resistivity, transmittance, and band gap energy of the CZO films.

Cu target power/W	Cu/at.%	Resistivity/Ω·cm	Transmittance/%	Band gap/eV
0	0	2.63	88.46	4.64
50	5.93	1.78	86.78	4.58
60	7.18	1.48	83.11	4.48
70	8.07	2.57	83.34	4.61

3.5. Optical properties

In order to further study the transmittances of the films, we prepare CZO films on glass substrates. Figure 5 shows the transmittances of the films with different Cu content in a wavelength range from 200 nm to 800 nm. As expected, all the films are transparent in the visible light region by exhibiting transmission above 81%, indicating that CZO films are of good transparency. High transmittance of the film indicates its low surface roughness and good homogeneity, which is in good agreement with SEM result of the film grown on glass substrates (not shown here). The average transmittance of the films decreases from 88.46% to 83.11% as the Cu content increases from 0 at.% to 7.18 at.%. The decrease in the transmittance value of the CZO film may be associated with the incident photons that are scattered by the metallic Cu crystals residing at substitutional positions of ZrO_2 host lattice and it may also be due to the lattice defects existing in ZrO_2 host lattice.[34] The similar observations on the different film samples with different dopants are made by the other researcher.[35] In addition, the sharp fall in transmittance observed at $\lambda \sim 350$ nm is due to the fundamental absorption edge of ZrO_2 which is caused by the light and occurrences of inter-band transitions. Moreover a shift in the absorption edge towards higher wavelength region is also observed.

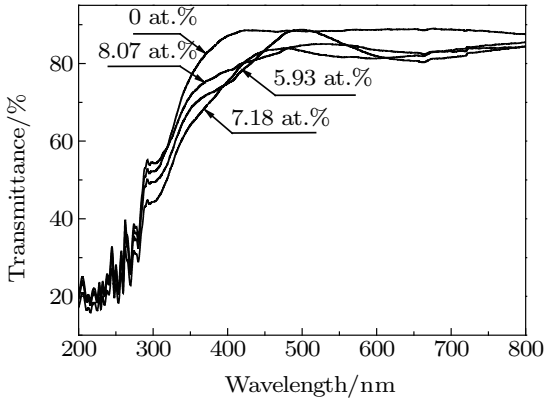


Fig. 5. UV–vis transmittance spectra of Cu-doped ZrO_2 films formed at various Cu doping content.

To understand the effect of Cu additions on the optical band gap of film, the $(\alpha h\nu)^2$ absorption coefficient (α^2) versus the photon energy $(h\nu)$ of Cu-doped ZrO_2 films are plotted in Fig. 6. The optical band gap (E_g) of film is verified for direct transition and can be determined from the following relationship:[21]

$$\alpha^2 = \alpha_0(h\nu - Eg), \tag{3}$$

where α_0 is the constant, $\alpha \propto \ln(1/T)$ the absorption coefficient, and T the transmittance of film.

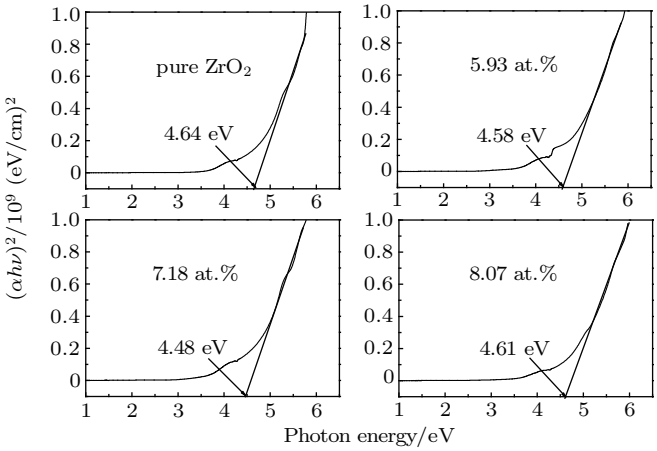


Fig. 6. $(\alpha h\nu)^2$ versus $(h\nu)$ curves of Cu-doped ZrO_2 films formed at various Cu doping content.

Then, E_g can be evaluated from the plot of α^2 versus $h\nu$, by using a linear fit of plots and extrapolating the linear part to photon energy axis at $\alpha^2 = 0$. The optical band gap values are 4.64, 4.58, 4.48, and 4.61 eV for 0, 5.93, 7.18, and 8.07 at.% CZO films, respectively (in Table 2). The optical band gap energies at low doping levels (5.93 at.% and 7.18 at.%), which could be due to band edge bending by Cu doping. In the case of Cu doping, Cu^{2+} ions are moved to the substituted sites in the ZrO_2 matrix and may act as a donor impurity. The doped Cu^{2+} ions increase the donor density and thus result in the formation of a donor level below the conduction band (tail-like states below the conduction band), thereby reducing the

band gap of ZrO_2.[36] However, further increasing Cu content to 8.07 at.%, the optical band gap is found to increase. This may be attributed to the presence of CuO phase.

4. Conclusions

In this work, Cu at various content of 0, 5.93, 7.18, and 8.07 at.% are successfully doped into ZrO_2 (CZO) films by direct current (DC) and radio frequency (RF) magnetron co-sputtering. The structural, electrical and optical properties are investigated each as a function of the Cu content in ZrO_2 film, determined by the power of Cu target. All these films have excellent crystalline quality with monocline structure, and crystal size becomes bigger after doping Cu. Moreover, both the average transmittance and band gap energy of the film decrease from 88.46% to 83.31% and from 4.64 eV to 4.48 eV, respectively, with the increase of doping content. The electrical resistivity of the film decreases with Cu doping increasing, indicating that the conductivity of ZrO_2 film is improved. The obtained results presented in this study strongly suggest that the CZO film is very appealing candidate for functional and smart devices.

References

[1] Reisfeld R, Zelner M and Patra A 2000 *J. Alloys Compd.* **300** 147151
[2] Pamu D, Sudheendran K, Krishna M G, Raju K C J and Bhatnagar A K 2009 *Thin Solid Films* **517** 15871591
[3] Lee W G, Cho K H, Lee S B, Park S B and Jang H 2009 *J. Alloys Compd.* **474** 268272
[4] Padmamalini N and Ambujam K 2014 *Superlattices Microstruct.* **76** 376384
[5] Khojier K, Savaloni H and Jafari F 2013 *J. Theor. Appl. Phys.* **7** 55
[6] Chakraborty S, Bera M K, Dalapathi G K, Paramanik D, Varma S, Bose P K, Bhattacharya S and Maiti C K 2006 *Semicond. Sci. Technol.* **21** 467472
[7] Ma C Y and Zhang Q Y 2008 *Vacuum* **82** 847851
[8] Hembram K P S S, Dutta G, Waghmare U V and Rao G M 2007 *Physica B* **399** 2126
[9] Zhang H H, Ma C Y and Zhang Q Y 2009 *Vacuum* **83** 13111316
[10] Septawendar R, Purwasasmita B S, Suhanda, Nurdiwijayanto L and Edwin F 2011 *J. Ceram. Process. Res.* **12** 110113
[11] Pakma O, Özdemir C, Kariper I A, Özaydın C and Güllü Ö 2016 *Appl. Surf. Sci.* **377** 159166
[12] Ray J C, Pramanik P and Ram S 2001 *Mater. Lett.* **48** 281291
[13] Xiao Q L, Xu C, Shao S Y, Shao J D and Fan Z X 2009 *Vacuum* **83** 366371
[14] Jeong J and Yong K 2003 *J. Cryst. Growth* **254** 6569
[15] Gordon G R, Becker J, Hausmann D and Suh S 2001 *Chem. Mater.* **13** 24632464
[16] Berlin I J and Joy K 2015 *Physica B* **457** 182187
[17] Sethi G, Sunal P, Horn M W and Lanagan M T 2009 *J. Vac. Sci. Technol. A* **27** 577583
[18] Thaveedeetrakul A, Witit-anun N and Boonamnuayvitay V 2012 *Appl. Surf. Sci.* **258** 26122619
[19] Kumar A, Dhiman P and Singh M 2016 *Ceram. Int.* **42** 79187923
[20] Bruns S, Vergöhl M, Werner O and Wallendorf T 2012 *Thin Solid Films* **520** 41224126
[21] Musil J, Sklenka J, Čerstvy R, Suzuki T, Mori T and Takahashi M 2012 *Surf. Coat. Technol.* **207** 355360
[22] Myagkov V G, Bykova L E, Bayukov O A, Zhigalov V S, Tambasov I A, Zharkov S M, Matsynin A A and Bondarenko G N 2015 *J. Alloys Compd.* **636** 223228
[23] Joy K 2014 *Thin Solid Films* **556** 99104
[24] Seidel S, Sabelfeld A, Strohmeyer R, Schreiber G, Klemm V, Rafaja D, Joseph Y and Heitmann J 2016 *Thin Solid Films* **606** 1318
[25] Korsunska N, Baran M, Polishchuk Y, Kolomys O, Stara T, Kharchenko M, Gorban O, Strelchuk V, Venger Y, Kladko V and Khomenkovaa L 2015 *ECS J. Solid State Sci. Technol.* **4** 103110
[26] Korsunska N, Polishchuk Y, Kladko V, Portier X and Khomenkova L 2017 *Mater. Res. Express* **4** 035024
[27] Mukhtar M, Munisa L and Saleh R 2012 *Mater. Sci. Appl.* **3** 543551
[28] Holzwarth U and Gibson N 2011 *Nat. Nanotechnol.* **6** 534
[29] Anitha V S, Lekshmy S S and Joy K 2016 *J. Alloys Compd.* **675** 331340
[30] Kumaravel R, Ramamurthi K, Sulania I, Asokan K and Kanjilal D 2011 *Radiat. Phys. Chem.* **80** 435439
[31] Schuetze A P, Lewis W, Brown C and Geerts W J 2004 *Am. J. Phys.* **72** 149153
[32] Sreedhar A, Kwon J H, Yi J, Kim J S and Gwag J S 2016 *Mater. Sci. Semicond. Process.* **49** 814
[33] Presto S, Viviani M 2016 *Solid State Ionics* **295** 111116
[34] Paraguay F, Yoshida M M, Morales J, Solis J and Estrada W 2000 *Thin Solid Films* **373** 137140
[35] Tarwal N L, Gurav K V, Mujawar S H, Sadale S B, Nam K W, Bae W R, Moholkar A V, Kim J H, Patil P S and Jang J H 2014 *Ceram. Int.* **40** 76697677
[36] Sandeep K M, Bhat S and Dharmaprakash S M 2017 *J. Phys. Chem. Solids* **104** 3644